Large quantum superpositions of a levitated nanodiamond through spin-optomechanical coupling

Zhang-qi Yin,[1,*] Tongcang Li,[2] Xiang Zhang,[2] and L. M. Duan[1,3]

[1]*The Center for Quantum Information, Institute for Interdisciplinary Information Sciences, Tsinghua University,*
Beijing 100084, People's Republic of China
[2]*NSF Nanoscale Science and Engineering Center, 3112 Etcheverry Hall, University of California, Berkeley, California 94720, USA*
[3]*Department of Physics, University of Michigan, Ann Arbor, Michigan 48109, USA*

We propose a method to generate and detect large quantum superposition states and arbitrary Fock states for the oscillational mode of an optically levitated nanocrystal diamond. The nonlinear interaction required for the generation of non-Gaussian quantum states is enabled through the spin-mechanical coupling with a built-in nitrogen-vacancy center inside the nanodiamond. The proposed method allows the generation of large superpositions of nanoparticles with millions of atoms and the observation of the associated spatial quantum interference under reasonable experimental conditions.

　　　　　　　PACS number(s): 03.75.−b, 03.65.Ta, 42.50.Dv, 42.50.Wk

I. INTRODUCTION

Creating spatial quantum superpositions with massive objects is one of the most challenging and attractive goals in macroscopic quantum mechanics [1–4]. It provides potential opportunities to experimentally test different wave-function collapse models [2], including gravity-induced state reduction [5], which is a manifestation of the apparent conflict between general relativity and quantum mechanics. Quantum superpositions and interferences have been realized with electrons, neutrons, atoms, and complex molecules with several hundred atoms [6]. Among different optomechanical systems [7–10], optically levitated dielectric particles in vacuum [11–21] are particularly promising for creating superposition states with the largest *macroscopicity* (as defined in Ref. [4]). Due to the absence of the mechanical contact in this system, the decoherence [22] can be negligible and the oscillation frequency is fully tunable. Once cooled to the quantum regime, optically trapped nanoparticles in vacuum will be ultrasensitive detectors [23–25] and can even be used to study self-assembly of the nanoparticles in vacuum [26,27]. To generate spatial quantum superpositions and other non-Gaussian states with an optical cavity, however, requires a very strong quadratic coupling [21,28]. This is a very demanding requirement. To enhance the quadratic coupling, Romero-Isart *et al.* [21] proposed to prepare spatial quantum superpositions of nanoparticles with two interconnected high-finesse optical cavities: one cavity for cooling and the other cavity for preparing the superposition state with a squared position measurement when the nanoparticle falls through it.

In this paper, we propose a scheme to generate and detect arbitrary Fock states and spatial quantum superposition states for the center-of-mass oscillation of an optically trapped nanocrystal diamond using the induced spin-optomechanical coupling. The nanodiamond has build-in nitrogen-vacancy (NV) centers, and electron spins associated with diamond NV centers make good qubits for quantum information processing as they have nice coherence properties even at room temperature [29]. With the assistance of a strong magnetic

field gradient from a nearby magnetic tip, strong coupling between the NV spin and the mechanical oscillation of the nanodiamond can be achieved. Using this coupling, we show how to generate arbitrary Fock states, entangled states, and large quantum superpositions for the nanodiamond. The generated spatial superposition states and other mesoscopic quantum superposition states can be detected through different spatial interference patterns of the nanodiamond.

II. THE PROPOSED SETUP

Nanodiamonds with NV centers have been recently trapped by optical tweezers in liquid [30,31] and atmospheric air [32], and similar technologies can be used to optically trap them in vacuum [16]. As shown in Fig. 1, we consider a nanodiamond of mass m optically trapped in vacuum with trapping frequency ω_m. The motion of its center-of-mass mode a_m is described by the Hamiltonian $H_m = \hbar \omega_m a_m^\dagger a_m$. The nanodiamond has a built-in NV center with its level configuration shown in Fig. 1(b) in the ground-state manifold. The NV spin is described by the Hamiltonian $H_{NV} = \hbar(\omega_{+1}|+1\rangle\langle+1| + \omega_{-1}|-1\rangle\langle-1|)$, where we have set $|0\rangle$ as the energy zero point. A magnet tip near the NV center induces a strong magnetic field gradient [33,34], which couples the electron spin and the center-of-mass oscillation of the nanodiamond. The coupling Hamiltonian is denoted by $H_{NVm} = \hbar \lambda S_z(a_m + a_m^\dagger)$ [35,36], where $S_z \equiv |+1\rangle\langle+1| - |-1\rangle\langle-1|$. The coupling strength $\lambda = g_s \mu_B G_m a_0/\hbar$, where $a_0 = \sqrt{\hbar/2m\omega_m}$, $g_s \simeq 2$ is the Landé g factor, μ_B is the Bohr magneton, and G_m is the magnetic field gradient along the NV center axis.

The nanodiamond is trapped inside an optical cavity to precool its center-of-mass motion to the ground state through the cavity-assisted cooling, as has been demonstrated for other mechanical systems [9]. The heating of the mechanical mode is negligible compared with the cavity-induced cooling rate as the Q factor for the center-of-mass oscillation of an optically levitated particle in vacuum is very high [11]. Note that the center-of-mass oscillation is not subject to the intrinsic dissipation of the material as it is decoupled from all the other mechanical modes and can be cooled to the ground state even if the diamond itself (its internal modes) is at room temperature.
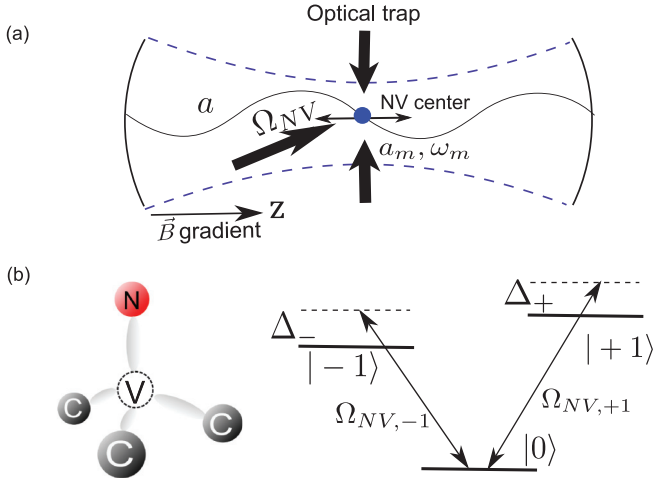
────────

*yinzhangqi@mail.tsinghua.edu.cn

FIG. 1. (Color online) (a) A nanodiamond with a NV center is optically trapped in vacuum with spin-mechanical coupling enabled through a nearby magnetic tip and optomechanical coupling through a cavity around. (b) The atomic structure (left) and the level diagram (right) in the ground-state manifold for a NV center in the nanodiamond.

An alternative way to achieve the ground-state cooling of the center-of-mass mode, although not demonstrated yet in experiments, is to use a combination of optical pumping of the NV spin state and fast exchange between the spin and the motional excitations [35]. In this case, we do not need any optical cavity, which can further simplify the experimental setup.

III. PREPARATION AND DETECTION OF FOCK STATES

In order to prepare the Fock states, we first cool the mechanical mode to the ground state. The NV spin is initially set to the state $|0\rangle$, which is decoupled from the mechanical mode during the cooling. Initialization and single shot detection of the NV spin have been well accomplished experimentally [37]. We assume that the NV center is at a position with zero magnetic field and a large field gradient. We apply a microwave drive with the Hamiltonian $H_{\mathrm{drive}} = \hbar(\Omega_{\mathrm{NV},+1}e^{i\omega_{l+}t}|0\rangle\langle+1| + \Omega_{\mathrm{NV},-1}e^{i\omega_{l-}t}|0\rangle\langle-1| + \mathrm{H.c.})/2$ and set the Rabi frequency $\Omega_{\mathrm{NV},\pm1} = \Omega_{\mathrm{NV}}$ and the detuning $\Delta_\pm \equiv \omega_{l\pm} - \omega_{\pm1} = \Delta$. With $\Delta \gg |\Omega_{\mathrm{NV}}|$, we adiabatically eliminate the level $|0\rangle$ and get the following effective Hamiltonian:

$$H_e = \hbar\omega_m a_m^\dagger a_m + \hbar\Omega\sigma_z + \hbar\lambda(\sigma_+ + \sigma_-)(a_m + a_m^\dagger), \quad (1)$$

where $\Omega = |\Omega_{\mathrm{NV}}|^2/4\Delta$, $\sigma_z = |+\rangle\langle+| - |-\rangle\langle-|$, $\sigma_+ = |+\rangle\langle-|$, $\sigma_- = |-\rangle\langle+|$, and we have defined the new basis states $|+\rangle = (|+1\rangle + |-1\rangle)/\sqrt{2}$, $|-\rangle = (|+1\rangle - |-1\rangle)/\sqrt{2}$. In the limit $\lambda \ll \omega_m$, we set $\Omega = \omega_m/2$ and use the rotating wave approximation to get an effective interaction Hamiltonian between the mechanical mode and the NV center spin, with the form

$$H_{\mathrm{JC}} = \hbar\lambda\sigma_+ a_m + \mathrm{H.c.}$$

This represents the standard Jaynes-Cummings (JC) coupling Hamiltonian. Similarly, if we set $\Omega = -\omega_m/2$, the anti-JC
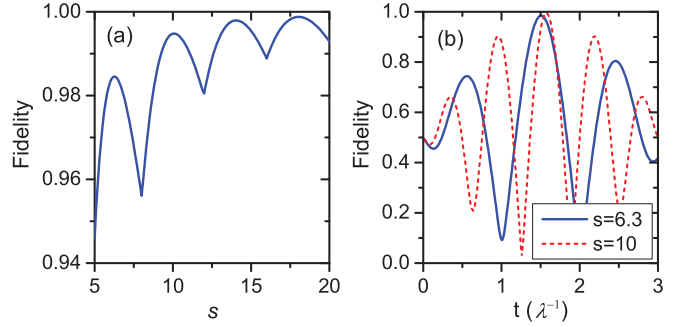

FIG. 2. (Color online) Fidelity of creating the phonon number superposition state $(|0\rangle_m + i|1\rangle_m)/\sqrt{2}$ by coherent-state transfer between the NV spin and the mechanical mode. Fidelities higher than 99% can be achieved. (a) The peak fidelity as a function of the parameter $s = \omega_m/\lambda$. (b) The fidelity as a function of the interaction time for two different parameters ($s = 6.3, 10$).

Hamiltonian can be realized with

$$H_{\mathrm{aJC}} = \hbar\lambda\sigma_+ a_m^\dagger + \mathrm{H.c.}$$

Arbitrary Fock states and their superpositions can be prepared with a combination of JC and anti-JC coupling Hamiltonians. For example, to generate the Fock state $|2\rangle_m$, we initialize the state to $|+\rangle|0\rangle_m$, turn on the JC coupling for a duration $t_1 = \pi/(2\lambda)$ to get $|-\rangle|1\rangle_m$, and then turn on the anti-JC coupling for a duration $t_2 = t_1/\sqrt{2}$ to get $|+\rangle|2\rangle_m$. The Fock state with arbitrary phonon number n_m can be generated by repeating the above two basic steps, and the interaction time is $t_i = t_1/\sqrt{i}$ for the ith step [38]. Superpositions of different Fock states can also be generated. For instance, if we initialize the state to $(c_0|+\rangle + c_1|-\rangle) \otimes |0\rangle_m/\sqrt{2}$ through a microwave with arbitrary coefficients c_0, c_1, and turn on the JC coupling for a duration t_1, we get the superposition state $|-\rangle \otimes (c_1|0\rangle_m + ic_0|1\rangle_m)/\sqrt{2}$. In Fig. 2(a), we plot the fidelity of the mechanical state as a function of the parameter $s = \omega_m/\lambda$ using the full Hamiltonian with rotating wave approximation. The fidelity oscillates with many local maxima and the envelope approaches unity when $s \gg 1$. In practice, we have a very high fidelity already by setting s at the local maxima such as 6.3 or 10.0. By using the optical cavity, the Fock state $|n_m\rangle_m$ of the mechanical mode can also be mapped to the corresponding Fock state of the output light field [25].

The effective Hamiltonian for the spin-phonon coupling takes the form

$$H_{\mathrm{QND}} = \hbar\chi\sigma_z a_m^\dagger a_m,$$

with $\chi = 4\Omega\lambda^2/(4\Omega^2 - \omega_m^2)$ when the detuning $||\Omega| - \omega_m/2| \gg \lambda$. The Hamiltonian H_{QND} can be used for a quantum nondemolition (QND) measurement of the phonon number: we prepare the NV center spin in a superposition state $|+\rangle + e^{i\phi}|-\rangle)/\sqrt{2}$, and the phase ϕ evolves by $\phi(t) = \phi_0 + 2\chi n_m t$, where $n_m = a_m^\dagger a_m$ denotes the phonon number. Through a measurement of the phase change, one can detect the phonon number.

The preparation and detection of the Fock states can all be done within the spin coherence time. Let us estimate the typical parameters. A large magnetic field gradient can be generated by moving the nanodiamond close to a magnetic

tip. A large field gradient up to 4×10^7 T/m has been reported near the write head of a magnetic disk drive [33]. In magnetic resonance force microscopy systems, the gradient of the order of 10^6 T/m has been realized [34]. Here we take the gradient $G = 10^5$ T/m and get the coupling $\lambda \simeq 2\pi \times 52$ kHz for a nanodiamond with the diameter $d = 30$ nm in an optical trap with a trapping frequency $\omega_m = 2\pi \times 0.5$ MHz. The Fock states and their superpositions can then be generated with a time scale $1/\lambda$ of about a few μs, and the QND detection rate $2|\chi| \sim 2\pi \times 25$ kHz with the detuning $||\Omega| - \omega_m/2| \sim 5\lambda$. The NV electron-spin dephasing time over 1.8 ms has been observed at room temperature [39], which is long compared with the Fock-state preparation time $1/\lambda$ and the detection time $1/(2|\chi|)$. The threshold gradient is 2×10^3 T/m for the trap frequency 0.5 MHz.

IV. GENERATION AND DETECTION OF LARGE SPATIAL SUPERPOSITION STATES

To prepare the spatial quantum superposition state, we need to generate the quantum superposition of the nanodiamond at distinct locations. Without the microwave driving, the spin-mechanical coupling Hamiltonian takes the form

$$H = \hbar\omega_m a_m^\dagger a_m + \hbar\lambda S_z(a_m + a_m^\dagger). \quad (2)$$

The mechanical mode is initialized to the vacuum state $|0\rangle_m$ (or a Fock state $|n_m\rangle_m$) in a strong trap with the trapping frequency ω_{m0} and the NV center spin is prepared in the state $|0\rangle$. Although the ground-state cooling is most effective in a strong trap, to generate large spatial separation of the wave packets it is better to first lower the trap frequency by tuning the laser intensity for the optical trap. While it is possible to lower the trap frequency through an adiabatic sweep to keep the phonon state unchanged, a more effective way is to use a nonadiabatic state-preserving sweep [40], which allows arbitrarily short sweeping time. We denote $|n_m\rangle_{m1}$ as the mechanical state in the lower frequency ω_{m1}. We then apply an impulsive microwave pulse to suddenly change the NV spin to the state $(|+1\rangle + |-1\rangle)/\sqrt{2}$ and simultaneously decrease the trap frequency to $\omega_{m2} \leqslant \omega_{m1}$. The evolution of the system state under the Hamiltonian (2) then automatically splits the wave packet for the center-of-mass motion of the nanodiamond (see the illustration in Fig. 3). The splitting attains the maximum at time $T_2/2 = \pi/\omega_{m2}$, where the maximum distance of the two wave packets in the superposition state is $D_m = 8\lambda a_2/\omega_{m2} = 4g_s\mu_B G/(m\omega_{m2}^2)$, where $a_2 = \sqrt{\hbar/2m\omega_{m2}}$. At this moment, the system state is

$$|\Psi_S\rangle = (|+1\rangle|D_m/2\rangle_{n_m} + |-1\rangle| - D_m/2\rangle_{n_m})/\sqrt{2}, \quad (3)$$

where $|\pm D_m/2\rangle_{n_m} \equiv (-1)^{a_m^\dagger a_m} e^{\pm D_m(a_m^\dagger - a_m)/4a_2}|n_m\rangle_1$ is the displaced Fock state (or coherent states when $n_m = 0$). This is just the entangled spatial superposition state, as discussed in Appendix A. In Figs. 3(d) and 3(e), we show the evolution of the splitting of the spatial wave packets for the nanodiamond under the initial vacuum $|0\rangle_m$ or Fock state $|1\rangle_m$. The maximum distance D_m is plotted in Fig. 4 versus trap frequency, magnetic field gradient, and diameter d of the nanodiamond, and superposition states with separation D_m comparable to
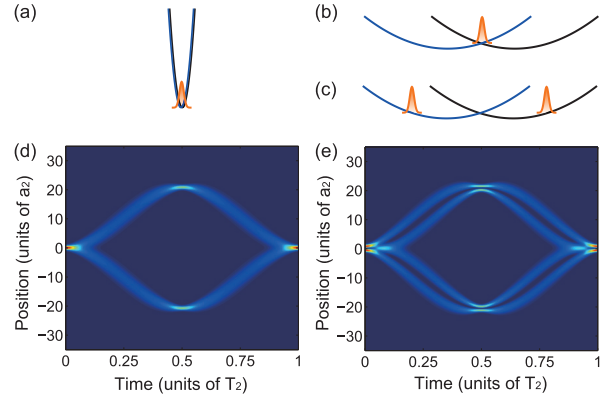

FIG. 3. (Color online) (a) A nanodiamond with $d = 30$ nm is confined tightly by a 100 kHz frequency optical tweezer in a magnetic field with a large gradient $G = 4 \times 10^4$ T/m. Its NV center is prepared in a state $|0\rangle$. (b) The power of the optical tweezer is suddenly reduced to 20 kHz, and the NV center is changed to a superposition state $(|+1\rangle + |-1\rangle)/\sqrt{2}$, while the magnetic gradient is the same. As a result, the trap centers for different electron spins are separated. (c) The nanodiamond changes into a spatial superposition state as the state evolves in time. (d) and (e) show the time evolution of the probability distribution of the nanodiamond after the trapping frequency and the NV center state are suddenly changed. The mechanical state is initially (d) $|0\rangle_{m,100\,\text{kHz}}$ or (e) $|1\rangle_{m,100\,\text{kHz}}$ in the high-frequency trap. $a_2 = \sqrt{\hbar/2m\omega_{m2}} = 0.092$ nm and $T_2 = 50$ μs.

or larger than the diameter d are achievable under realistic experimental conditions.

To transform the entangled cat state $|\Psi_S\rangle$ to the standard cat state $|\psi_\pm\rangle_{n_m} \equiv (|D_m/2\rangle_{n_m} \pm |-D_m/2\rangle_{n_m})/\sqrt{2}$, we need to apply a disentangling operation to conditionally flip the NV spin using displacement of the diamond as the control qubit. This can be achieved as different displacements of the wave packet induce relative energy shifts of the spin levels due to the applied magnetic field gradient. As an estimate, for the example we considered in Fig. 5 (with a 30-nm-diameter diamond in a 20 kHz trap under a magnetic gradient of 3×10^4 T/m), the spin energy splitting is about
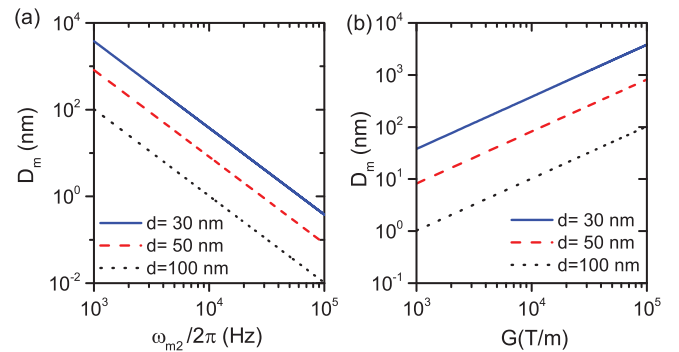

FIG. 4. (Color online) (a) Maximum spatial separation D_m of the superposition state as a function of trap frequency ω_{m2} when the magnetic gradient is 10^5 T/m. (b) Maximum spatial separation D_m as a function of the magnetic gradient G when the trapping frequency is 1 kHz. Macroscopic superposition states with separation larger than the size of the particle can be achieved with a moderate magnetic gradient.
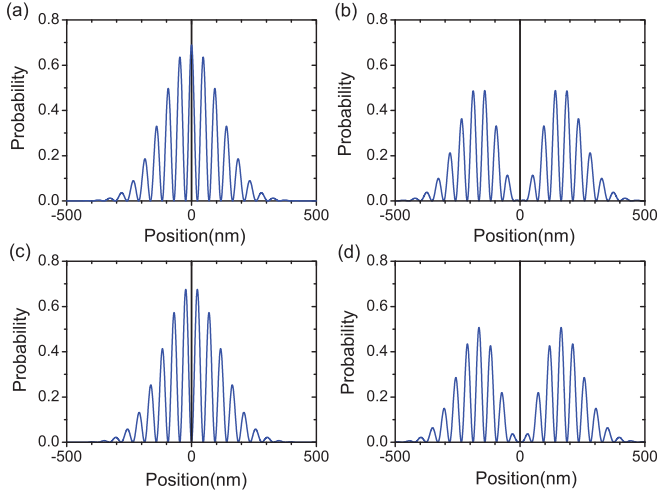
FIG. 5. (Color online) Spatial interference patterns for a 30 nm nanodiamond after 10 ms of free expansion. The nanodiamond is initially prepared in the vacuum state $|0\rangle_m$ or the one-phonon state $|1\rangle_m$ of a 20 kHz trap. The magnetic gradient is 3×10^4 T/m. Before the trap is turned off, the center of mass of the nanodiamond is prepared in (a) $|\psi_+\rangle_0$, (b) $|\psi_+\rangle_1$, (c) $|\psi_-\rangle_0$, and (d) $|\psi_-\rangle_1$.

2.4 MHz between the $|+1\rangle|D_m/2\rangle_{n_m}$ and $|-1\rangle|-D_m/2\rangle_{n_m}$ components, which is much larger than the typical transition linewidth of the NV spin (in the order of kHz). So we can apply first an impulsive microwave pulse to transfer the component state $|+1\rangle|D_m/2\rangle_{n_m}$ to $|0\rangle|D_m/2\rangle_{n_m}$ without affecting $|-1\rangle|-D_m/2\rangle_{n_m}$, and then another pulse to transfer $|-1\rangle|-D_m/2\rangle_{n_m}$ to $\pm|0\rangle|-D_m/2\rangle_{n_m}$. After the two pulses, the spin state gets disentangled and the position of the diamond is prepared in the quantum superposition state $|\psi_\pm\rangle_{n_m}$.

To detect the spatial superposition state, we can turn off the optical trap and let the spatial wave function freely evolve for some time t. The split wave packets will cause interference just like Young's double-slit experiment. The period of the interference pattern is $\Delta z = 2\pi\hbar t/(mD_m)$ (Appendix B). As an estimation of typical parameters, we take $\omega_{m1} = \omega_{m2} = 2\pi \times 20$ kHz, $d = 30$ nm, and magnetic field gradient 3×10^4 T/m. The spin-phonon coupling rate $\lambda \simeq 2\pi \times 77$ kHz and the maximum distance $D_m \simeq 31a_2$. The preparation time of the superposition state is about 25 μs, which is much less than the coherence time of the NV spin. For the time-of-flight measurement after turning off the trap, we see the interference pattern with a period of 47 nm after $t = 10$ ms, as shown in Fig. 5, which is large enough to be spatially resolved [14–16]. In experiments, the initial state is the thermal state with $\langle n_m \rangle \ll 1$, which can be approximated by the vacuum and the first Fock state. By combining the interference pattern of vacuum and $|1\rangle_m$ state with its thermal weight, we can get the interference pattern for the $n_m \ll 1$ thermal state. As show in Fig. 6, because the weight of $|1\rangle_m$ is $n_m \ll 1$, the final interference pattern is very close to the vacuum one. In other words, the interference pattern is robust for the thermal phonon number.

V. DISCUSSION AND CONCLUSION

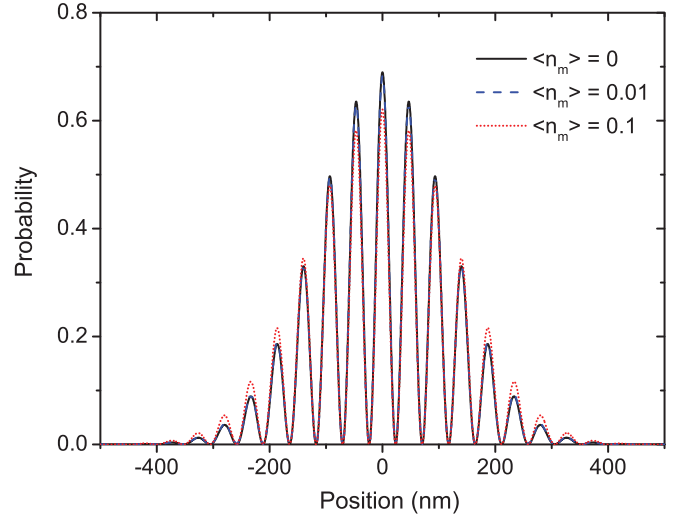Finally, we briefly mention the source of decoherence for preparation of the spatial quantum superposition state. The

FIG. 6. (Color online) Spatial interference patterns for a 30 nm nanodiamond after 10 ms of free expansion. The magnetic gradient is 3×10^4 T/m. The nanodiamond is initially prepared in the thermal state of a 20 kHz trap. Before the trap is turned off, the center of mass of the nanodiamond is prepared in the spatial quantum superposition state with initial thermal phonon number $\langle n_m \rangle = 0, 0.01, 0.1$.

decoherence of the cat state by photon scattering is negligible during the time-of-flight measurement as the laser is turned off. The main source of decoherence includes background gas collision and blackbody radiation. Using the formula

$$\gamma_s = 4\pi\sqrt{2\pi}Pd^2/(\sqrt{3}\bar{v}m_a)$$

from Ref. [21], we estimate that the decoherence rate due to the background gas collision is about 8 Hz under the condition that the vacuum pressure $P \sim 10^{-11}$ Torr, the mass of the molecule $m_a = 4.83 \times 10^{-26}$ kg, and the gas temperature $T_b \sim 4.5$ K. Here, $\bar{v} = \sqrt{8k_B T/(\pi m_a)}$ is the mean velocity of the molecule and k_B is the Boltzmann constant. This rate is small compared with the experimental time scale of 10 ms. As the internal temperature T_i of the diamond is typically much higher than the background gas temperature T_b, the blackbody radiation is dominated by the thermal photon emission from the diamond, which is $\gamma_{bb,e} = (2\pi^5/189)cd^3(k_BT_i/\hbar c)^6 \text{Im}[(\epsilon_{bb}-1)/(\epsilon_{bb}+2)]z^2$ [21]. Here, c is the light-speed constant, ϵ_{bb} is the permittivity of diamond for the blackbody radiation, and z is the interference width. The frequency of the thermal photon is of the order of THz. Compared with the silica sphere considered in [21], the emission rate of THz photons is smaller by about two orders of magnitude for the diamond. Even with T_i at room temperature, the decoherence rate γ_{bb} due to the thermal photon emission is estimated to be only 3 Hz for our proposed scheme. In addition, with the built-in electronic states of the NV center, the internal temperature of the diamond can be reduced through laser cooling [41]. As $\gamma_{bb} \propto T_i^6$, this allows further significant suppression of the decoherence rate. For the current discussion of a 30 nm particle in the 0.5 MHz trap, the gravity-induced decoherence is estimated to be of the order of 10^{-62} Hz for the superposition of Fock states [42], and 10^{-7} Hz for spatial superposition states with displacement 30 nm [5], and can be neglected. Our proposed scheme is more relevant for testing objective collapse models [21].

We note that the same scheme could also apply to other optically levitated nanoparticles with built-in electron spins, such as [28]Si nanoparticles with donor spins [43] or nanocrystals doped with rare-earth ions [44]. This scheme thus opens up the possibility to observe large quantum superpositions for mesoscopic objects under realistic experimental conditions and to test predictions of quantum mechanics in unexplored regions.

APPENDIX A: DERIVATION OF ENTANGLED SPATIAL SUPERPOSITION STATE

The Hamiltonian (2) in rotating frame with $H_0 = \hbar\omega_m a_m^\dagger a_m$ reads $H_I = \hbar S_z \lambda(a e^{-i\omega_m t} + \text{H.c.})$. The unitary operator in the rotating frame is $U_I = \mathcal{T} \exp[-\frac{i}{\hbar}\int H_I(t)dt]$, which can be solved with Magnus expansion $U_I = \exp[\sum_k \Omega_k(t)]$. Here,

$$\Omega_1 = -\frac{i}{\hbar}\int_0^t H_I(t_1)dt_1$$
$$= \frac{S_z\lambda}{\omega_m}[(e^{-i\omega_m t}-1)a - (e^{i\omega_m t}-1)a^\dagger], \quad \text{(A1)}$$

and

$$\Omega_2 = -\frac{1}{2}\int_0^t\int_0^{t_1}[H_I(t_1),H_I(t_2)]dt_1 dt_2$$
$$= i\lambda^2\left[\frac{t}{\omega_m} - \frac{\sin(\omega_m t)}{\omega_m^2}\right]. \quad \text{(A2)}$$

For $k \geqslant 3$, Ω_k are always equal to zero. Neglecting the global phase Ω_2, we get $U_I = \exp[\alpha(t)a - \alpha(t)^* a^\dagger]$, where $\alpha(t) = S_z\lambda(e^{-i\omega_m t}-1)/\omega_m$. Back to the original frame, we get $U_I' = e^{-i\omega_m a_m^\dagger a_m t}U_I$. Specifically, at the time of half period with trap frequency $\omega_m = \omega_{m_2}$, we find that $U_I' = (-1)^{a_m^\dagger a_m}\exp[S_z D_m(a_m^\dagger - a_m)/4a_2]$, where $D_m = 4g_s\mu_B G/(m\omega_{m_2}^2)$, and $a_2 = \sqrt{\hbar/(2m\omega_{m_2})}$. The entangled spatial state can be calculated as $|\Psi_S\rangle = U_I'|n_m\rangle_{m1}$.

APPENDIX B: PERIOD OF INTERFERENCE PATTERN

We suppose that the superposition of the displacement state is $|\psi_+\rangle_0 = [\varphi_{0L}(z) + \varphi_{0R}(z)]/\sqrt{2}$, where $\varphi_{0R}(z) = \frac{\sqrt{\beta}}{\pi^{1/4}}e^{-\beta^2(z-b)^2/2}$, $\varphi_{0L}(z) = \frac{\sqrt{\beta}}{\pi^{1/4}}e^{-\beta^2(z+b)^2/2}$, and $\beta = \sqrt{m\omega_2/\hbar} = 1/(\sqrt{2}a_2)$. b is the displacement of the original wave function. After the Fourier transfer, the right-branch wave function becomes

$$\varphi_{0L}(k) = \frac{1}{\pi^{1/4}\sqrt{\beta}}e^{-ibk-(k^2/2\beta^2)}.$$

The Fourier transfer of the left branch of the wave function can be calculated with a similar method. The time evolution of the wave function is

$$\varphi_0(z,t) = \frac{1}{\sqrt{2\pi}}\int_{-\infty}^{+\infty}dk\,\varphi(k)e^{i(kz-\omega t)},$$

where $\omega = \hbar k^2/2m$. We suppose that z is in the unit of $1/\beta$, t is in the unit of $2m/\hbar\beta^2$, and k is in the unit of β. The probability distribution of the wave function is

$$\varphi_0^*(z,t)\varphi_0(z,t) = \frac{1}{2\sqrt{\pi(1+4t^2)}}\left[e^{-\frac{(z-b)^2}{1+4t^2}} + e^{-\frac{(z+b)^2}{1+4t^2}} + 2e^{-\frac{z^2+b^2}{1+4t^2}}\cos\left(\frac{4bzt}{1+4t^2}\right)\right].$$

The interference period is $\Delta z = 2\pi(1+4t^2)/(4bt)$. For the long-time limit $bt \gg 1$, we have $\Delta z = 2\pi t/b$. In our paper, we have $D_m = 2b$. Therefore, in the SI unit, the interference period is $\Delta z = 2\pi\hbar t/(mD_m)$.

[1] K. Hornberger, S. Gerlich, P. Haslinger, S. Nimmrichter, and M. Arndt, Rev. Mod. Phys. **84**, 157 (2012).

[2] A. Bassi, K. Lochan, S. Satin, T. P. Singh, and H. Ulbricht, Rev. Mod. Phys. **85**, 471 (2013).

[3] Yanbei Chen, J. Phys. B: At. Mol. Opt. Phys. **46**, 104001 (2013).

[4] S. Nimmrichter and K. Hornberger, Phys. Rev. Lett. **110**, 160403 (2013).

[5] R. Penrose, Gen. Relativ. Gravit. **28**, 581 (1996).

[6] C. Davisson and L. H. Germer, Nature (London) **119**, 558 (1927); I. Estermann and O. Stern, Z. Phys. **61**, 95 (1930); W. Schöllkopf and J. P. Toennies, Science **266**, 1345 (1994); M. Kasevich and S. Chu, Phys. Rev. Lett. **67**, 181 (1991); C. Monroe *et al.*, Science **272**, 1131 (1996); M. Arndt *et al.*, Nature (London) **401**, 680 (1999); S. Gerlich *et al.*, Nat. Commun. **2**, 263 (2011).

[7] I. Wilson-Rae, N. Nooshi, W. Zwerger, and T. J. Kippenberg, Phys. Rev. Lett. **99**, 093901 (2007).

[8] F. Marquardt, J. P. Chen, A. A. Clerk, and S. M. Girvin, Phys. Rev. Lett. **99**, 093902 (2007).

[9] A. D. O'Connell *et al.*, Nature (London) **464**, 697 (2010); Jasper Chan *et al.*, *ibid.* **478**, 89 (2011); J. D. Teufel *et al.*, *ibid.* **475**, 359 (2011).

[10] M. Aspelmeyer, T. J. Kippenberg, and F. Marquardt, arXiv:1303.0733.

[11] D. E. Chang *et al.*, Proc. Natl. Acad. Sci. USA **107**, 1005 (2010).

[12] O. Romero-Isart, M. Juan, R. Quidant, and J. Cirac, New J. Phys. **12**, 033015 (2010).

[13] O. Romero-Isart, A. C. Pflanzer, M. L. Juan, R. Quidant, N. Kiesel, M. Aspelmeyer, and J. I. Cirac, Phys. Rev. A **83**, 013803 (2011).

[14] T. Li, S. Kheifets, D. Medellin, and M. G. Raizen, Science **328**, 1673 (2010).

[15] Tongcang Li, Simon Kheifets, and Mark G. Raizen, Nat. Phys. **7**, 527 (2011).

[16] J. Gieseler, B. Deutsch, R. Quidant, and L. Novotny, Phys. Rev. Lett. **109**, 103603 (2012).

[17] T. S. Monteiro *et al.*, New J. Phys. **15**, 015001 (2013).

[18] A. C. Pflanzer, O. Romero-Isart, and J. I. Cirac, Phys. Rev. A **86**, 013802 (2012).

[19] H. K. Cheung and C. K. Law, Phys. Rev. A **86**, 033807 (2012).

[20] Nikolai Kiesel *et al.*, arXiv:1304.6679.

[21] O. Romero-Isart, A. C. Pflanzer, F. Blaser, R. Kaltenbaek, N. Kiesel, M. Aspelmeyer, and J. I. Cirac, Phys. Rev. Lett. **107**, 020405 (2011); O. Romero-Isart, Phys. Rev. A **84**, 052121 (2011).

[22] Zhang-qi Yin, Phys. Rev. A **80**, 033821 (2009).

[23] A. A. Geraci, S. B. Papp, and J. Kitching, Phys. Rev. Lett. **105**, 101101 (2010).

[24] A. Arvanitaki and A. A. Geraci, Phys. Rev. Lett. **110**, 071105 (2013).

[25] Zhang-qi Yin, Tongcang Li, and M. Feng, Phys. Rev. A **83**, 013816 (2011).

[26] W. Lechner, S. J. M. Habraken, N. Kiesel, M. Aspelmeyer, and P. Zoller, Phys. Rev. Lett. **110**, 143604 (2013).

[27] S. J. M. Habraken, W. Lechner, and P. Zoller, Phys. Rev. A **87**, 053808 (2013).

[28] J. D. Thompson *et al.*, Nature (London) **452**, 72 (2008).

[29] J. Wrachtrup and F. Jelezko, J. Phys.: Condens. Matter **18**, S807 (2006).

[30] V. R. Horowitz *et al.*, Proc. Natl. Acad. Sci. USA **109**, 13493 (2012).

[31] M. Geiselmann *et al.*, Nat. Nanotechnol. **8**, 175 (2013).

[32] Levi P. Neukirch *et al.*, Opt. Lett. **38**, 2976 (2013).

[33] C. Tsang *et al.*, IEEE Trans. Magn. **42**, 145 (2006).

[34] H. J. Mamin *et al.*, Nat. Nanotechnol. **2**, 301 (2007).

[35] P. Rabl, P. Cappellaro, M. V. Gurudev Dutt, L. Jiang, J. R. Maze, and M. D. Lukin, Phys. Rev. B **79**, 041302(R) (2009).

[36] S. Kolkowitz *et al.*, Science **335**, 1603 (2012).

[37] L. Robledo, L. Childress, H. Bernien, B. Hensen, P. F. A. Alkemade, and R. Hanson, Nature (London) **477**, 574 (2011).

[38] D. M. Meekhof, C. Monroe, B. E. King, W. M. Itano, and D. J. Wineland, Phys. Rev. Lett. **76**, 1796 (1996).

[39] G. Balasubramanian *et al.*, Nat. Mater. **8**, 383 (2009).

[40] X. Chen, A. Ruschhaupt, S. Schmidt, A. del Campo, D. Guéry-Odelin, and J. G. Muga, Phys. Rev. Lett. **104**, 063002 (2010).

[41] Denis V. Seletskiy *et al.*, Nat. Photon. **4**, 161 (2010); Jun Zhang *et al.*, Nature (London) **493**, 504 (2013).

[42] M. P. Blencowe, Phys. Rev. Lett. **111**, 021302 (2013).

[43] M. Steger *et al.*, Science **336**, 1280 (2012).

[44] W. Tittel *et al.*, Laser Photon. Rev. **4**, 244 (2010).